Numerical Analysis on the Mechanism of Blast Mitigation by Water Droplets

Kakeru Shibue [1], Yuta Sugiyama [2] & Akiko Matsuo [3]

[1] Graduate School of Science and Technology, Keio University, 3-14-1 Hiyoshi, Kohoku, Yokohama, Kanagawa 223-8522, Japan, kakeru1017@keio.jp

[2] Research Institute of Science for Safety and Sustainability, National Institute of Advanced Industrial Science and Technology, Central 5, 1-1-1 Higashi, Tsukuba, Ibaraki 305-8565, Japan, yuta.sugiyama@aist.go.jp

[3] Department of Mechanical Engineering, Keio University, 3-14-1 Hiyoshi, Kohoku, Yokohama, Kanagawa 223-8522, Japan, matsuo@mech.keio.ac.jp

ABSTRACT

Hydrogen has a high risk of ignition owing to its extremely low ignition energy and wide range of flammability. Therefore, acquiring parameters relating to safe usage is of particular interest. The ignition of hydrogen generates combustion processes such as detonation and deflagration, which may produce a blast wave. The severity of injuries sustained from a blast wave is determined by its strength. To reduce the physical hazards caused by explosion, there is a need for some concepts for attenuating explosions and blast waves. In the present study, we used water droplets as a material to reduce the blast wave strength. Numerical analysis of the interaction between blast waves and water droplets in a shock tube was conducted to understand the mitigation mechanism of blast wave. In this report, we numerically modelled the experiment conducted by Mataradze et al. [1] to understand the main factor of blast mitigation by water droplets. In order to quantitatively clarify the mitigation effect of water droplets on the blast wave especially by quasi-steady drag, here we conducted parameter studies on water droplet sprayed region. From this calculation, it was suggested that the location of water droplet sprayed layer did not affect the blast mitigation effect at far side of the high explosives.

1.0 INTRODCTION

Explosion phenomenon is defined as a process in which the pressure rises rapidly due to chemical or physical causes, and the gas expands with explosion sound. Hydrogen is a substance with the potential to cause very large explosions. Therefore, acquiring parameters relating to safe usage of hydrogen is of particular interest. Hydrogen itself and its combustion products are completely nontoxic, so it is expected to alternate fossil fuels which are thought to be bad for the environment. On the other hand, hydrogen has a high risk of ignition owing to its extremely low ignition energy and wide range of flammability. So if the explosion accident by hydrogen occurs unexpectedly, it may cause severe damage to both humans and surrounding buildings. For example, on May 23, 2019, a large-scale hydrogen explosion accident occurred. As a result, two people died and six people injured in the eastern city of Gangneung in South Korea. [2]

Explosion damage should be the worst condition when considering detonation instead of deflagration. In this case, we can replace detonation with the explosion of a high explosive. [3] So in this paper, the explosion of a high explosive was used as one way to model a hydrogen explosion.

Initiation of a high explosive generates extremely high-temperature, high-pressure, and high-velocity detonation products and a shock wave in the air. This shock wave adiabatically heats and compresses the air and induces air motion. Figure 1 shows a typical pressure waveform of a spherical blast wave at a certain point. The pressure rises rapidly from the atmospheric pressure P_0 due to the shock wave and reaches the peak overpressure P_s. The pressure of the air behind the shock wave decreases due to the

expansion wave because the shock wave expands spherically from the explosion point. The pressure eventually reaches below atmospheric pressure and returns to atmospheric pressure P_0 again by the inflow of air. When discussing the effects of a blast wave, the extent of the damage to both the human and structures depends on the blast wave parameters such as the peak overpressure P_s. Therefore, it is considered that mitigating peak overpressure leads to reduction of explosion damage. So far, various researches for mitigating the blast wave have been investigated by interacting with various materials and the blast wave. [4][5]

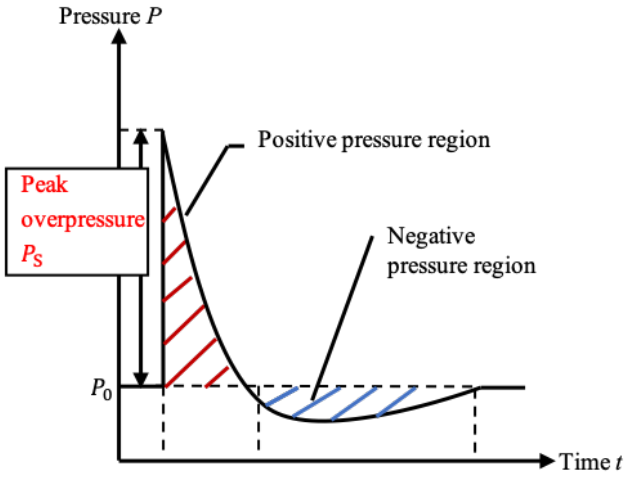

Figure 1. Characteristic blast wave pressure profile at a certain point

There have been many studies using water for blast mitigation. In a previous study by Cheng et al. [6], they conducted numerical analyses to understand the effect of the blast mitigation when the explosive was surrounded by water (water wall). Numerical analyses showed that the blast pressure was mitigated due to transition from the blast energy to the water wall. It was also found that the blast mitigation effect increased as the weight of water increased. In an experiment conducted by Tamba et al. [7] in which water droplets were sprayed around an explosive, it was shown that the blast mitigation effect increases as the amount of water droplets increased and sprinkled area decreased. In these studies, the weight for water wall is responsible for the blast mitigation, whereas, there are many parameters such as droplet diameter, distribution density, distance between explosives and water droplets to determine the effect of the blast mitigation by water droplets. Due to various parameters described above, quantitative blast mitigation mechanism has not been elucidated. At the present stage, it is thought that the blast energy is mitigated by converting the energy of the blast wave into kinetic energy and internal energy of the blast mitigation material such as water. [8] It has been suggested that adiabatic compression by shock waves causes temperature rise and acceleration of air, and that heat transfer or momentum exchange when it interacts with water droplets and heat absorption by evaporation are effective in the blast mitigation. [9-10] However, the contribution of these factors to the mitigation effect is not clear. In this paper, we will discuss in detail about drag force in particular.

In this study, numerical analysis modelling the experiment conducted by Mataradze et al. [1] was performed. They detonated an explosive in a shock tube, and a one-dimensional blast wave was utilized to interact with the water droplets. They measured the pressure time histories to estimate the mitigation effect of the water droplets on the blast wave. It was shown that the effect of the blast mitigation varied depending on the spray position of water droplets. However, quantitative evaluation of the blast mitigation was still inadequate. Therefore, we numerically attempt quantitative evaluation of the blast mitigation by water droplets focusing on quasi-steady drag between the blast wave and water droplets.

2.0 NUMERICAL METHOD AND COMPUTATIONAL TARGET

2.1 Governing equation and numerical method

2.1.1 The governing equation for gas phase

The governing equations for the gas phase are the volume-averaged two-dimensional compressible Euler equation considering the porosity and source term for interactions between gas and droplets. The equations for mass conservation, momentum conservation, energy conservation, and conserving the mass fraction of each gas species are shown below:

$$\frac{\partial}{\partial t}\left(\alpha_{\mathrm{g}}\rho_{\mathrm{g}}\right)+\nabla\cdot\left(\alpha_{\mathrm{g}}\rho_{\mathrm{g}}\mathbf{u}_{\mathrm{g}}\right)=0, \tag{1}$$

$$\frac{\partial}{\partial t}\left(\alpha_{\mathrm{g}}\rho_{\mathrm{g}}\mathbf{u}_{\mathrm{g}}\right)+\nabla\cdot\left(\alpha_{\mathrm{g}}\rho_{\mathrm{g}}\mathbf{u}_{\mathrm{g}}\mathbf{u}_{\mathrm{g}}\right)+\alpha_{\mathrm{g}}\nabla p_{\mathrm{g}}=-\mathbf{f}_{\mathrm{gp}}, \tag{2}$$

$$\frac{\partial}{\partial t}\left(\alpha_{\mathrm{g}}e_{\mathrm{g}}\right)+\nabla\cdot\left\{\alpha_{\mathrm{g}}\left(e_{\mathrm{g}}+p_{\mathrm{g}}\right)\mathbf{u}_{\mathrm{g}}\right\}+p_{\mathrm{g}}\frac{\partial}{\partial t}\alpha_{\mathrm{g}}=-s_{\mathrm{gp}}, \tag{3}$$

$$\frac{\partial}{\partial t}\left(\alpha_{\mathrm{g}}\rho_{\mathrm{g}}Y_{\mathrm{g,k}}\right)+\nabla\cdot\left(\alpha_{\mathrm{g}}\rho_{\mathrm{g}}Y_{\mathrm{g,k}}\mathbf{u}_{\mathrm{g}}\right)=0,\quad\sum_{\mathrm{k}=1}^{\mathrm{N}}Y_{\mathrm{g,k}}=1\,. \tag{4}$$

Here, the subscripts g and gp indicate physical quantities for the gas phase and interaction term between gas and water droplets respectively. α_{g}, ρ_{g}, $\mathbf{u}_{\mathrm{g}}$, p_{g} and e_{g} indicate the porosity (volume fraction), the density, the velocity vector, the pressure, and the total energy, respectively, for the gas phase. $Y_{\mathrm{g,k}}$ represents the mass fraction of gaseous species k (k=1 for oxygen and k=2 for nitrogen). The gas phase used in this analysis is air with a molar fraction of O_2:N_2 = 1:3.76. $\mathbf{f}_{\mathrm{gp}}$, s_{gp} indicate fluid force vector, transferred energy by the fluid force between gas and water droplets, respectively. The gas is assumed to be a calorically perfect gas, and the equation of state of the ideal gas shown by the following equation was used.

$$p_{\mathrm{g}}=\rho_{\mathrm{g}}RT_{\mathrm{g}} \tag{5}$$

R represents the gas constant.

2.1.2 The governing equation for droplets

The governing equations for each particle consist of the equations of motion for translation, energy conservation and number density conservation equation. In the computational target, the temperature gradient inside the particles is ignored because the Biot number is sufficiently small. The governing equations are shown below. In this analysis, a representative particle model is used for particle calculation. In the representative particle model, it is assumed that multiple particles are grouped together as a particle group i, and that the real particles included in the particle group behave the same as the representative particles. In addition, the representative particle is located at the center of the representative region, and the calculation of the fluid drag force, energy transfer by drag is performed at representative particle point:

$$\frac{d\mathbf{x}_{\mathrm{p,i}}}{dt}=\mathbf{u}_{\mathrm{p,i}}, \tag{6}$$

$$m_{\mathrm{p,i}}\frac{d\mathbf{u}_{\mathrm{p,i}}}{dt}=\mathbf{f}_{\mathrm{drag,i}}+V_{\mathrm{p,i}}\nabla p_{\mathrm{g}}=\mathbf{F}_{\mathrm{p-g,i}}, \tag{7}$$

$$\frac{dn_{\mathrm{p,i}}}{dt}=\dot{n}_{\mathrm{p,i}}. \tag{8}$$

Here, the subscript p indicates physical quantities for the water droplets phase. $\mathbf{x}_{\mathrm{p,i}}$, $m_{\mathrm{p,i}}$, $\mathbf{u}_{\mathrm{p,i}}$, $n_{\mathrm{p,i}}$, and $\dot{n}_{\mathrm{p,i}}$ are represent the position vector of the center of gravity, mass, translation speed, number density, and production rate for number density of i-th particle, respectively. The source term in Eq. 7 considers the gas phase pressure gradient force vector $V_{\mathrm{p,i}}\nabla p_{\mathrm{g}}$ and the fluid drag force vector $\mathbf{f}_{\mathrm{drag,i}}$. $V_{\mathrm{p,i}}$ is the particle volume, and $\mathbf{F}_{\mathrm{p-g,i}}$ is the sum of these fluid forces. The droplet breakup is taken into account. It occurs under the assumption that the droplet diameter decreases linearly during the breakup process. The critical Weber number and non-dimensional total breakup time are modelled following Brodkey [11] and Pilch and Erdman [12].

In the present study, we considered the quasi-steady drag for the fluid drag force:

$$\mathbf{f}_{\mathrm{drag,i}} = \frac{\pi}{8} n_{\mathrm{p,i}} \rho_{\mathrm{g}} d_{\mathrm{p,i}}^2 C_{\mathrm{d}} \left|\mathbf{u}_{\mathrm{g}} - \mathbf{u}_{\mathrm{p,i}}\right| \left(\mathbf{u}_{\mathrm{g}} - \mathbf{u}_{\mathrm{p,i}}\right). \tag{9}$$

This quasi-steady drag force is activated by the blast wave and water droplets. We focused on this force because the relative velocity is an important parameter in the present system, where the air velocity behind the blast wave is large and the blast mitigation is caused by the interaction with stationary water droplets.

In Eq. 9, $d_{\mathrm{p,i}}$ and C_{d} are the diameter of droplet and drag coefficient. The drag coefficient C_{d} in Eq. 10 is a function of the particle Reynolds number proposed by Jourdan et al. [13]. This model of Jourdan et al. was obtained for a wide range of particle Reynolds number in the experiments where water droplets interact with the flow behind the shock wave. Equation 10 was also used by Chauvin et al. [14] for a similar research target of the present study.

$$\log_{10}(C_{\mathrm{d}}) = -0.695 + 1.259\left(\log_{10}\left(\mathrm{Re}_{\mathrm{p,i}}\right)\right) - 0.464\left(\log_{10}\left(\mathrm{Re}_{\mathrm{p,i}}\right)\right)^2 + 0.045\left(\log_{10}\left(\mathrm{Re}_{\mathrm{p,i}}\right)\right)^3 \tag{10}$$

The particle Reynolds number is defined by the following equation:

$$\mathrm{Re}_{\mathrm{p,i}} = \frac{\rho_{\mathrm{g}} d_{\mathrm{p,i}} \left|\mathbf{u}_{\mathrm{g}} - \mathbf{u}_{\mathrm{p,i}}\right|}{\mu_{\mathrm{g}}}. \tag{11}$$

The interaction terms between the gas phase and particle are expressed by the following equations:

$$\mathbf{f}_{\mathrm{gp}} = \frac{1}{A_{\mathrm{cell}}} \sum_{\mathrm{i=1}}^{\mathrm{N}} \mathrm{n}_{\mathrm{p,i}}^{\mathrm{z}} \mathbf{F}_{\mathrm{p-g,i}}, \tag{12}$$

$$s_{\mathrm{gp}} = \frac{1}{A_{\mathrm{cell}}} \sum_{\mathrm{i=1}}^{\mathrm{N}} \mathrm{n}_{\mathrm{p,i}}^{\mathrm{z}} \mathbf{F}_{\mathrm{p-g,i}} \cdot \mathbf{u}_{\mathrm{p,i}}, \tag{13}$$

The fluid drag forces considered in this analysis are the pressure gradient force and the quasi-steady drag. $\mathrm{n}_{\mathrm{p,i}}^{\mathrm{z}}$ represents the number of actual particles existing in the unit depth of each particle group named ‘parcel’, and is determined to satisfy the following equation:

$$\alpha_{\mathrm{g}} = 1 - \alpha_{\mathrm{s}} = 1 - \frac{1}{A_{\mathrm{cell}}} \sum_{\forall_{\mathrm{i}} \in \mathrm{cell}} \mathrm{n}_{\mathrm{p,i}}^{\mathrm{z}} V_{\mathrm{p,i}}\,. \tag{14}$$

Here, α_{s} and A_{cell} represent the volume fraction of particles and the cell size area of structured grid.

For the discretization of the convection term, SLAU2 [15] with third order MUSCL interpolation [16] and van Albada limiter [17] was used. The time integration method for the gas phase and for particles

is third-order TVD Runge-Kutta method and symplectic Euler method, respectively. The calculations were performed ignoring gravity and lift forces.

2.2 Validation study

For studying the blast wave propagation numerically, we validate the present numerical method by modeling the experiment by Mataradze et al. [1] In this experiment, a spherical explosive was detonated in a shock tube, and they observed the interaction of the planar blast wave with water droplets. This phenomenon can be simplified as a one-dimensional blast wave-water water droplets interaction problem. Therefore, we perform numerical analyses with a simple computational target as shown in Fig. 2. For the initial condition, high-pressure air is placed near the wall of shock tube to model the high-pressure detonation products used in the experiment. The amount of high-pressure air is estimated by using the diluted high-pressure shock tube model by Sugiyama et al. [18] In this model, the energy of 5-g hexogen is obtained from the 1.38 times the energy of TNT (4.18 MJ/kg), and the length of this high-pressure air is set to 18 mm as equivalent to the explosive diameter. As a result, the pressure and temperature with 3.39 MPa and 4504 K calculated from the 5−g hexogen are modelled for the high-pressure area. For the gas except for the high-pressure area, the pressure and temperature of the air are fixed as 101325 Pa and 294 K, respectively.

As shown in Fig. 2, $x = 0$ m is placed at the position 0.5 m from the left end wall of the shock tube for the same coordinate system of the experiment. Therefore, the high-pressure gas region locates at $-0.5\ \text{m} \leq x \leq -0.482$ m.

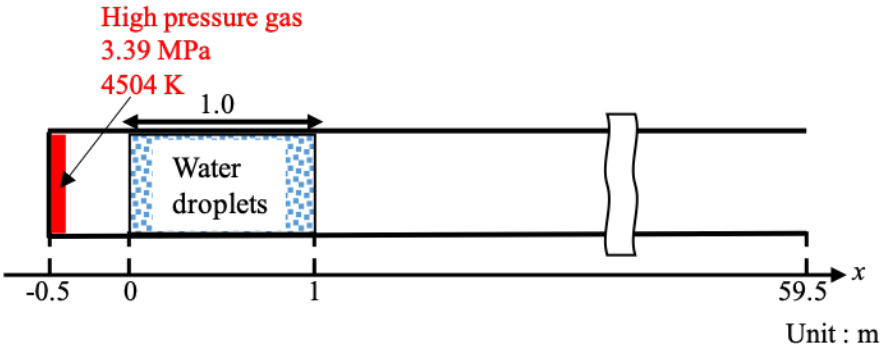

(a) The case of water droplets are sprayed at $0\ \text{m} < x < 1$ m

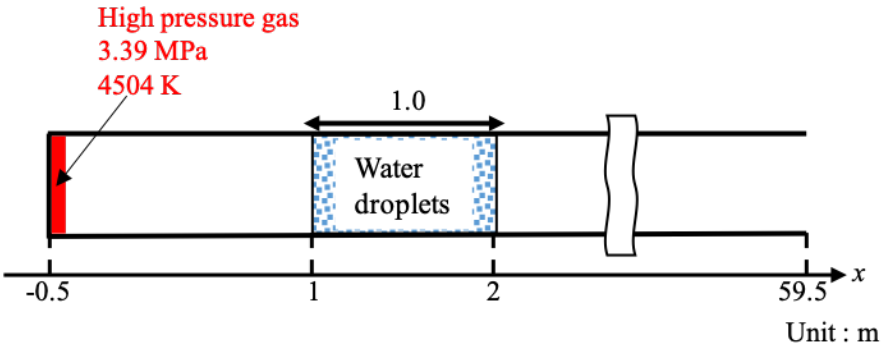

(b) The case of water droplets are sprayed at $1\ \text{m} < x < 2$ m

Figure 2. schematic images of the computational target

The computational grid used is an orthogonal grid with a constant grid width of 1 mm. The 0^{th}-order outflow boundary is applied to the exit in the x-direction, and the 2^{nd}-order mirror boundary is used for

the wall at $x = -0.5$ m. and 1st-order mirror boundary is used for both sides in the y-direction. Because of the one-dimensional problem, we assume that the length of the y-direction does not affect the numerical results, and the length of 1 mm in y-direction is set. Table 1 shows the conditions of water droplets. From the experimental measurement by Mataradze et al., the representative particle diameter was estimated around 143 μm. Then, in the present study, the particle size is constant at 143 μm for all particles. Because there is no description for the volume fraction of water droplets in their paper, we should determine the volume fraction to fit their experimental results. Here, we use the value of 0.27% for the volume fraction. To solve for spherical particles that are uniformly distributed in the z-direction with two-dimensional calculation, the parcel is modelled as a cylinder extending in the z-direction which is perpendicular to the xy plane.

Table 1. Particle conditions

Real particle diameter [μm]	143
Parcel diameter [μm]	143
Number of Parcel [/m]	1000
Number of water droplets in unit length in z-direction [1/m]	1763
Density [kg/m^3]	997
Volume fraction [%]	0.27

In the validation study, we compare the overpressure reduction coefficient K defined as following equation in their paper for the case when water droplets are sprayed at 0 m < x < 1 m as shown in Fig. 2a as

$$K = \frac{\Delta P_{\mathrm{a}} - \Delta P_{\mathrm{m}}}{\Delta P_{\mathrm{a}}}, \tag{15}$$

where ΔP_{a} and ΔP_{m} is peak overpressure without water droplets and with water droplets at the same distance from the high explosive. Figure 3 shows the relationship between K and distance x. From Fig. 3, we summarized the values and the average of K measured at the same points as in the experiment in Table 2. There are some errors for the value of K at each point between numerical result and experimental result, but the average of K matches well between them. From this result, we can confirm that the numerical model and conditions are appropriate for the study of the interaction between the blast wave and water droplets.

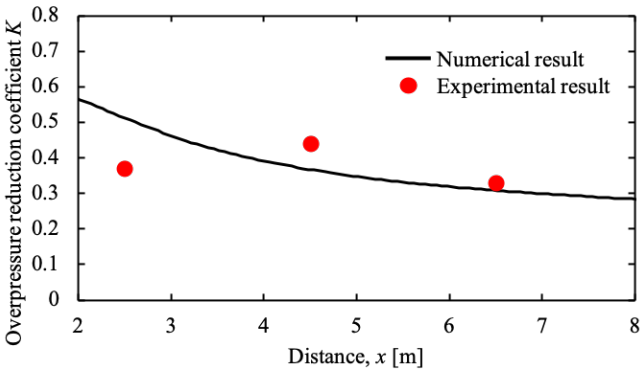

Figure 3. The relationship between K and distance between numerical and experimental results

Table 2. The value and the average of K in numerical and experimental results

Distance from the high explosive	The value of K in the experiment	The value of K in numerical calculation	The average of K in both the experiment and numerical calculation
2.5	0.37	0.49	0.38
4.5	0.44	0.35	
6.5	0.33	0.30	

2.3 Computational target and numerical conditions

The interactions between the gas and droplets considered in this analysis is quasi-steady drag. Therefore, numerical analysis is performed in two cases as shown in Table 3 by using the same computational target and conditions described in section 2.3. In Table 3, w/ and w/o denote that we include and do not include the condition described in the first row of Table 3, respectively, as Case 1 not considering water droplets, Case 2 considering water droplets with quasi-steady drag. We compare with the peak overpressure of two cases and attempt to consider the effect of quasi-steady drag. In next section, we investigated the peak overpressure mitigated by quasi-steady drag, and attempt to scale the peak overpressure to organize the effect of quasi-steady drag on the blast mitigation.

We examine how the effect of quasi-steady drag changes according to water droplet sprayed region, so water droplets are uniformly distributed in various regions, $0\ \text{m} < x < 1\ \text{m}$, $1\ \text{m} < x < 2\ \text{m}$, $2\ \text{m} < x < 3\ \text{m}$, $5\ \text{m} < x < 6\ \text{m}$, and $10\ \text{m} < x < 11\ \text{m}$. In Fig. 2a and 2b, we describe the situation when water droplets are sprayed at $0\ \text{m} < x < 1\ \text{m}$ and $1\ \text{m} < x < 2\ \text{m}$, respectively. Hereinafter, x_0 is defined as the start distance of the water droplet sprayed region.

Table 3. Two cases analyzed in this paper

Case	Water droplets	Quasi-steady drag
1	w/o	w/o
2	w/	w/

3.0 RESULTS AND DISCUSSION

In this section, we discuss the mitigation effect of the peak overpressure according to water droplet sprayed region and consider the scaling of peak overpressure by quasi-steady drag.

3.1 Peak overpressure distribution according to water droplet sprayed region

First, we investigated how the peak overpressure distribution changes according to water droplet sprayed region. Figure 4 shows peak overpressure distribution according to water droplet sprayed region. This graph indicates the maximum overpressures at each position during the whole time in the calculation. From Fig. 4, the peak overpressure clearly mitigated when the blast wave was passing through the water droplets layer. The constant region for the peak overpressure was computed, and the peak overpressures differ according to water droplet sprayed region behind and in the vicinity of the water droplet sprayed region. As the blast wave propagates further, the peak overpressure approaches to a single line, except for the case where $x_0 = 0$ m. We will explain the reason for the different behavior of $x_0 = 0$ m case later.

From this result, we will organize the effect of quasi-steady drag on the blast mitigation by scaling the peak overpressure in the following sections.

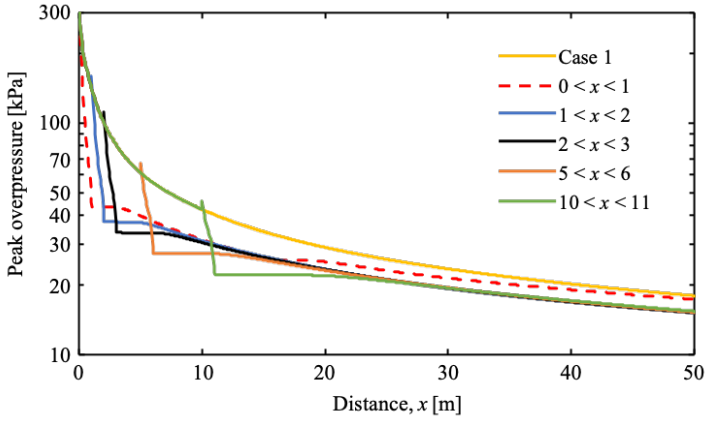

Figure 4. Peak overpressure distribution according to water droplet sprayed region

3.2 Scaling of peak overpressure distribution

3.2.1 Method of scaling

In this section, we attempt to capture the effect of quasi-steady drag on the blast mitigation by scaling. We perform to scale the blast pressure distribution and the spray region of water droplets by focusing on the fact that the quasi-steady drag mitigates the blast pressure. We took a similar method of scaling as Chauvin et al. [19] As a scaling method for the blast pressure distribution, we introduce the normalized peak overpressure distribution P(X). The blast pressure distribution $p_2(x)$ in Case 2 is normalized with respect to the blast pressure distribution $p_1(x)$ in Case 1. As a result, P(x) is defined as following equation.

$$\mathrm{P}(x) = \frac{p_2(x)}{p_1(x)} \tag{16}$$

The starting point in each water droplet sprayed region is set to x_0, respectively. X defined by following equation is used as the standard water droplet sprayed region.

$$X = x - x_0 \tag{17}$$

We got normalized peak overpressure by using P(x) and X.

3.2.2 Performance of scaling

By above procedure, we obtained the normalized peak overpressure distribution, as shown in Fig. 5. Figure 5a and 5b shows the normalized peak overpressure distributions for 0 m $\leq X \leq$ 10 m and 0 m $\leq X \leq$ 50 m. As shown in Fig. 5a, the normalized peak overpressure distribution can be smaller when water droplets are sprayed nearer the high explosives around X = 1 m. This is thought to be because the momentum loss of the gas phase due to quasi-steady drag is higher near the high explosives. Since the sum of the momentum of the water droplets corresponds to the total momentum loss in the gas phase, we show the total amount of momentum of water droplets in Fig. 6. In Fig. 6, the closer the region for interaction with the strong blast wave, the larger the maximum value of the total momentum of water droplets shown by symbol. The momentum of water droplets is induced by the flow behind the blast wave, but after enough time, it becomes zero. Figure 7 shows the relationship between the minimum value of normalized peak overpressure in Fig. 5a at X = 1 m and the maximum value of the total momentum of water droplets shown by symbol in Fig. 6. From Fig. 7, the closer the water droplet sprayed region is to the high explosives, the greater the momentum loss, and the smaller the minimum value of the normalized peak overpressure.

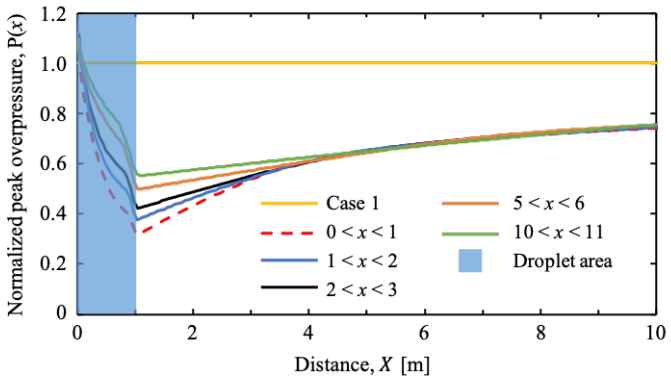

(a) When focusing only on the vicinity of the high explosives

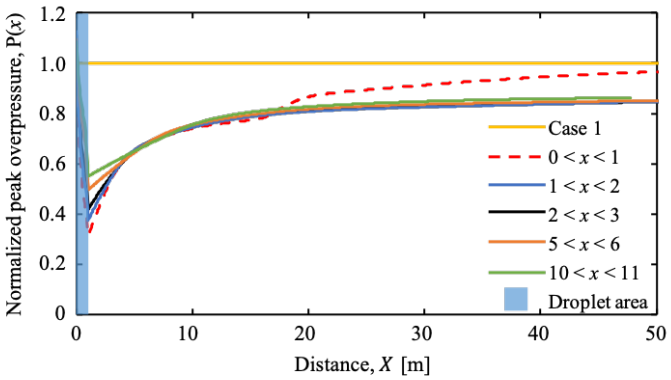

(b) When focusing on the far side of the high explosives

Figure 5. Normalized peak overpressure distribution according to water droplet sprayed region

In Fig, 5b, the normalized peak overpressure can be grouped after $X = 4.5$ m according to X, except for the case where $x_0 = 0$ m shown by dashed line. This suggests that under groupable conditions, the blast mitigation effect is independent of the location of the water droplets sprayed region, regardless of the behavior of the time history on the momentum loss in Fig. 6.

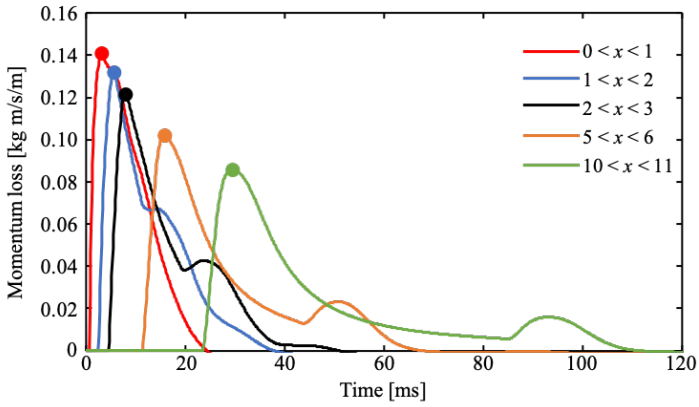

Figure 6. Time histories of momentum loss of the gas phase

(Symbol : Maximum value of the total momentum of water droplets for each case)

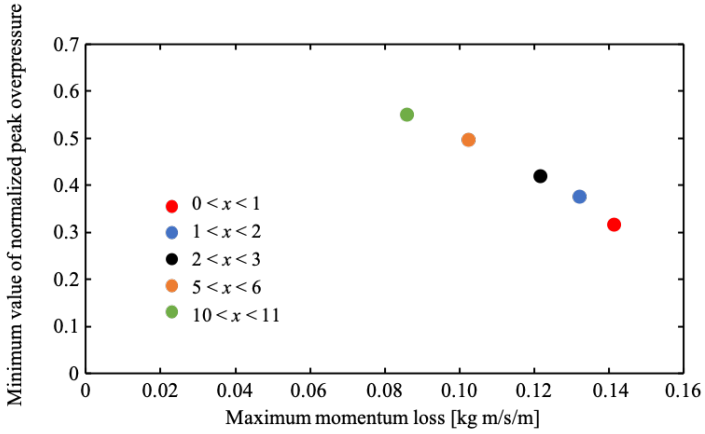

Figure 7. The relationship between the minimum value of normalized peak overpressure in Fig. 5a and maximum value of the total momentum loss of the gas phase in symbols of Fig. 6.

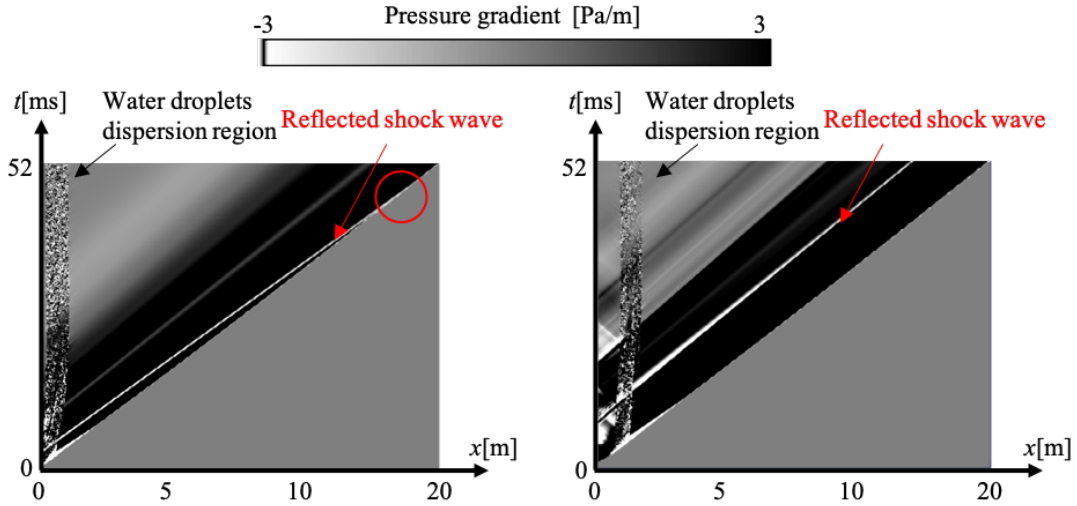

(a)Water droplets were sprayed 0 m < x < 1 m (b)Water droplets were sprayed 1 m < x < 2 m

Figure 8. x-t diagram of the pressure gradient

To consider why the normalized peak overpressure distribution behaves differently only when x_0 = 0 m, we illustrated the x-t diagram of the pressure gradient from the numerical results when water droplets are sprayed at 0 m < x < 1 m and 1 m < x < 2 m as shown in Fig. 8a and 8b, respectively. In Fig. 8a, the reflected wave generated by the interaction between the water droplets and the blast wave catches up with the preceding shock wave at around x = 18 m (Red circle in Fig. 8a). On the other hand, this phenomenon does not occur in the case when water droplets are sprayed at 1 m < x < 2 m in Fig. 8b. Therefore, the reflected wave is considered to be the cause of the pressure increase in the case of x_0 = 0 m. The normalized peak overpressure showed the additional increase around X = 18 m in this case. To maintain the blast mitigation effect even far side of the high explosives, it is necessary to spray water droplets at locations where pressure recovery due to the reflected shock wave does not appear.

4.0 CONCLUSIONS

In this paper, numerical analysis on the blast mitigation effect of water droplets was conducted, and we investigated the effect of quasi-steady drag. As a result, following information was obtained.

- The peak overpressure distribution due to quasi-steady drag can be evaluated with a single line regardless of the water droplet sprayed region by appropriately scaling.

- In the vicinity of the high explosives, the closer the region of the water droplet is to the high explosives, the greater momentum loss and has more mitigation effect. On the other hand, in the far side from the high explosives, the same mitigation effect converges regardless of the water droplet sprayed region.

- In order to maintain the blast mitigation effect even far side of the high explosives, it is necessary to spray water droplets at locations where pressure recovery due to the reflected shock wave does not appear.

REFERENCES

1. Mataradze, E., Chikhradze, N., Bochorishvili, N., Akhvlediani, I. and Tatishvili, D., Experimental Study of the Effect of Water Mist Location On Blast Overpressure Attenuation in A Shock Tube. IOP Conference Series: Earth Environmental Science, **95**: 042031, 2017.
2. The Korea Times, Hydrogen tank explosion kills 2 in Gangneung. https://www.koreatimes.co.kr/www/nation/2019/05/281_269400.html (accessed 24 June, 2021)
3. Mukhim, E. D., Abbasi, T., Tauseef, S. M. and Abbasi, S. A., A method for the estimation of overpressure generated by open air hydrogen explosions. *Journal of Loss Prevention in the Process Industries*, **52**, 2018, pp. 99-107.
4. Homae, T., Wakabayashi, K., Matsumura, T. and Nakayama, Y., Attenuation of blast wave using sand around a spherical pentolite. *Science and Technology of Energetic Materials*, **68**, No.3, 2007, pp. 90-93.
5. Pontalier, Q., Lhoumeau, M., Milne, A. M., Longbottom, A. W. and Frost, D. L. Numerical investigation of particle-blast interaction during explosive dispersal of liquids and granular materials. *Shock Waves*, **28**, No.3, 2018, pp. 513–531.
6. Cheng, M., Hung, K. C. and Chong, O. Y., Numerical study of water mitigation effects on blast wave. *Shock Waves*, **14**, No.3, 2005, pp. 217-223.
7. Tamba, T., Sugiyama, Y., Ohtani, K. and Wakabayashi, K., Experimental investigation of blast wave pressure mitigation by water droplets interaction. *Science and Technology of Energetic Materials*, **81**, No. 1, 2020, pp. 29-32.
8. Ananth, R., Willauer, H. D., Farley, J. P. and Williams, F. W., Effects of fine water mist on a confined blast. *Fire Technology*, **48**, No.3, 2012, pp. 641-675.
9. Cao, X., Wang, Z., Lu, Y. and Wang, Y., Numerical simulation of methane explosion suppression by ultrafine water mist in a confined space. *Tunnelling and Underground Space Technology*, **109**, No. 5: 103777, 2021.
10. Schwer, D. A. and Kaliasanath, K., Numerical simulations of the mitigation of unconfined explosions using water-mist. *Proceedings of the Combustion Institute*, **31**, No.2, 2007, pp. 2361-2369.
11. Brodkey, R. S., The Phenomena of Fluid Motions, 1967, Addison-Wesley, Reading Mass.
12. Pilch, M., Erdman, C. A., Use of break-up time data to predict the maximum size of stable fragment for acceleration induced breakup of a liquid drop. *International Journal of Multiphase Flow*, **13**, No. 6, 1987, pp. 741–757.
13. Jourdan, G., Houas, L., Igra, O., Estivalezes, J.L., Devals, C. and Meshkov, E.E., Drag coefficient of a sphere in a non-stationary flow: new results. *Proceedings of The Royal Society A*, **463**, No. 2088, 2007, pp. 3323–3345.
14. Chauvin, A., Daniel, E., Chinnayya, A. and Jourdan, G., Shock waves in sprays: numerical study of secondary atomization and experimental comparison. *Shock Waves*, **26**, No. 4, 2016, pp. 403-415.

15. Kitamura, K. and Shima, E., Towards shock-stable and accurate hypersonic heating computations: A new pressure flux for AUSM-family schemes. *Journal of Computational Physics*, **245**, No. 15, 2013, pp. 62-83.
16. van Leer, B., Toward the ultimate conservative difference scheme. Ⅳ, A New approach to numerical convection. *Journal of Computational Physics*, **23**, No. 3, 1977, pp. 276-299.
17. van Albada, G. D., van Leer, B. and Roberts Jr., W., A comparative study of computational methods in cosmic gas dynamics. *Astronomy and Astrophysics*, **108**, No. 1, 1982, pp. 76-84.
18. Sugiyama, Y., Wakabayashi, K., Matsumura, T. and Nakayama, Y., Numerical estimation of blast wave strength from an underground structure. *Sci. Tech. Energetic Materials*, **76**, No. 1, 2015, pp. 14-19.
19. Chauvin, A., Jourdan, G., Daniel, E., Hauas, L. and Tosello, R., Experimental investigation of the propagation of a planar shock wave through a two-phase gas-liquid medium. *Physics of Fluid*, **23**, No. 11: 113301, 2011.